Nonlinear Dyn
https://doi.org/10.1007/s11071-024-10667-y

RESEARCH

Effects of seasonal hunting and food quantity variations on the Lotka-Volterra model

Attila Genda · Alexander Fidlin · Stefano Lenci · Oleg Gendelman

Received: 1 August 2024 / Accepted: 15 November 2024

Abstract The Lotka-Volterra model is instrumental for understanding the dynamic interactions between predator and prey populations, especially as human activities like habitat destruction, pollution, and climate change rapidly alter living environments, making it more important than ever to understand the underlying mechanisms that drive population changes and to predict and mitigate the impacts of human interventions on wildlife populations. In this study, we investigate how periodic hunting and variations in food quantity impact the classical Hamiltonian Lotka-Volterra model. We do this by modeling variations in the prey reproduction rate with a periodically varying coefficient. We aim to understand how the system responds to these periodic disturbances and to identify the conditions under which the population sizes undergo significant oscillations. Our findings suggest that specific frequencies of hunting or food quantity variations can drive populations out of equilibrium to dangerously low levels, increasing the risk of extinction. The analysis is based on perturbation methods, primarily addressing the 1:1 resonance and using action-angle variables to simplify the system into new canonical coordinates. The results have significant implications for understanding and managing biological systems, offering insights that can aid in preserving species by identifying critical hunting thresholds and frequencies. We also give estimates for the time period of the Lotka-Volterra model in the vicinity of the nontrivial equilibrium and very far from the equilibrium.

Keywords Lotka-Volterra model · Level-crossing · Action-angle coordinates · Resonance · Transient process · Population dynamics · Hamiltonian systems

A. Genda (✉) · A. Fidlin
Institute of Engineering Mechanics, Karlsruhe Institute of Technology, Karlsruhe, Germany
e-mail: attila.genda@kit.edu

A. Fidlin
e-mail: alexander.fidlin@kit.edu

S. Lenci
Department of Civil Engineering, Building and Architecture, Polytechnic University of the Marche, Ancona, Italy
e-mail: s.lenci@staff.univpm.it

O. Gendelman
Mechanical Engineering, Technion - Israel Institute of Technology, Haifa, Israel
e-mail: ovgend@technion.ac.il

1 Introduction

The dynamic interactions between species in ecosystems are complex and often involve both consumption and predation. One of the foundational models used to study these interactions is the Lotka-Volterra model, which captures predator–prey dynamics through differential equations [1]. Originally developed by *Alfred J. Lotka* in 1920 [2] and independently by *Vito Volterra* in 1926 [3], this model has been instrumental in understanding how species populations vary over time due to their interactions.

Published online: 05 December 2024

The Lotka-Volterra equations describe how the population of a prey species grows exponentially in the absence of predators and how the predator population declines in the absence of prey. When these species interact, the model predicts oscillatory dynamics in which the predator population lags behind the prey population, resulting in cyclical variations [2,3]. These works laid the foundation for a vast body of research exploring various extensions and modifications of the model to better reflect ecological systems in the real world [1,4–8].

The model not only attracted the attention of biologists and ecologists, but also prompted mathematicians to start working on it and its generalizations. A significant extension to the classical Lotka-Volterra model involves incorporating time-varying coefficients to account for periodic environmental changes, such as seasonal hunting, variations in food availability, or settling and migration of species.

In [9], a decomposition-aggregation framework using vector Lyapunov functions was proposed for stability analysis of Lotka-Volterra equations. Equations with nonlinear time-varying coefficients were studied to derive stability conditions for nonnegative equilibria and analyze ultimate boundedness of motions.

Redheffer made significant theoretical contributions by providing conditions under which the Lotka-Volterra equations have unique and stable solutions in a generalized n-dimensional case with time-dependent model coefficients, rigorously proving the reliability of the model [10,11]. However, because of its general nature, his work is very theoretical and cannot be directly applied to practical calculations.

Táboas investigated the bifurcations of periodic solutions in a periodically forced Lotka-Volterra predator–prey model, focusing on the principal 1:1 resonance [12]. The study demonstrated that under specific conditions, the system exhibits exactly two T-periodic solutions near the singular point, highlighting the unique dynamics induced by the periodic forcing.

In [13], the authors numerically investigated the periodic harvesting of one or both predator–prey species, pointing out that the Lotka-Volterra model with periodic harvesting is essential for integrated farming systems because it helps optimize production and maintain sustainability, allowing farmers to manage better systems where, for example, vegetables are prey and fish are predators, thus maximizing the benefits of combining crops with livestock [14,15].

It is well known that the Lotka-Volterra equations have a Hamiltonian structure and admit a conservation law [16]. *Plank* [17] explores the Hamiltonian structure of the Lotka-Volterra equations in both two-dimensional and n-dimensional cases, aiming to construct all possible Hamiltonian functions for the two-dimensional Lotka-Volterra equations and extend these functions to the n-dimensional case by choosing an appropriate Poisson structure, with the main result that Hamiltonian functions used in the two-dimensional case can also be applied to the n-dimensional case, providing a unified approach to analyzing the Hamiltonian dynamics of Lotka-Volterra systems across different dimensions.

The canonical formalism using action-angle (AA) variables is a powerful tool in dynamical systems theory, especially for analyzing Hamiltonian systems [18–21]. These variables have played a crucial role in the derivation of important results such as the theory of adiabatic invariants [18], the Kolmogorov-Arnold-Moser theorem [20,22,23] and the canonical perturbation theory [20,23].

This approach is efficient for studying both autonomous and non-autonomous Hamiltonian systems, particularly in the vicinity of the primary resonance. Transforming the system into AA variables simplifies the averaged differential equations by deriving an additional conservation law, which allows analytical calculation of solutions and provides deeper insight into the system's behavior [24]. This method is particularly useful for describing slow-fast processes and analyzing whether the motion escapes a specific region of the phase space or leads to the crossing of some predefined level of a system observable.

Recent research by *Gendelman et al.* has focused on the dynamics of Hamiltonian systems, exploring how periodic perturbations can lead to escape phenomena [25–29].

In this study, we investigate the impact of periodic hunting and variations in food quantity on the Lotka-Volterra model by introducing a periodically varying coefficient. By modeling these disturbances, we aim to understand how specific frequencies of hunting or food quantity variations can drive populations out of equilibrium, potentially leading to extinction. Our analysis employs perturbation methods, focusing on the 1:1 resonance and using AA variables to simplify the system into new canonical coordinates. The findings of this study have significant implications for the preser-

vation of species, providing insights that can aid in the management of biological systems more effectively. By identifying the frequency-dependent critical amplitude variations of the prey reproduction rate, our research offers valuable guidance for ecological management and conservation efforts.

This article is structured as follows. Section 2 presents the classical Lotka-Volterra equations and defines the level-crossing problem. In Sect. 3, we reduce the problem by first transforming the equations into AA variables, followed by averaging under the assumption of 1:1 resonance. The averaged equations yield a new integral of motion, which is used to calculate the critical forcing amplitude depending on the excitation frequency. In Sect. 4, we compare the analytical results with the numerical ones. Finally, Sect. 5 concludes the work and provides scope for further research. In the Appendix, additional results concerning the time period of the unperturbed Lotka-Volterra model are presented under the assumptions of small or very large deviations from the equilibrium.

2 Problem setting

We investigate the Lotka-Volterra equations of the following form:

$$\frac{dX}{d\tau} = \tilde{\alpha}(t)X - \tilde{\beta}XY, \tag{1}$$

$$\frac{dY}{d\tau} = \tilde{\gamma}XY - \tilde{\delta}Y, \tag{2}$$

where X and $Y \in \mathbb{R}_0^+$ denote the prey and predator population size, respectively. We assume that $\tilde{\beta}, \tilde{\gamma}, \tilde{\delta} \in \mathbb{R}_0^+$. We introduce the nondimensional variables x and y and the nondimensional time t as follows

$$x := \frac{\tilde{\gamma}}{\tilde{\delta}}X, \quad y := \frac{\tilde{\beta}}{\tilde{\delta}}Y, \quad t := \tilde{\delta}\tau, \tag{3}$$

Equations (1) can be rewritten as

$$\frac{dx}{dt} = \alpha(t)x - xy, \qquad \text{with } \alpha(t) := \frac{\tilde{\alpha}(t)}{\tilde{\delta}} \tag{4}$$

$$\frac{dy}{dt} = xy - y. \tag{5}$$

We assume that the nondimensional reproduction rate of the prey species varies harmonically with time, including a positive bias, that is, $\alpha(t) = \alpha_0 - f\sin(\omega t + \beta)$ with $\alpha_0 \in \mathbb{R}_0^+$.

We are interested in the dynamics of this system, starting at the non-trivial equilibrium

$$x_0 = 1, \qquad y_0 = \alpha_0, \tag{6}$$

which has the linearized angular eigenfrequency

$$\Omega := \sqrt{\alpha_0}. \tag{7}$$

We define the critical and dangerously small population sizes x_{crit} and y_{crit} for both species. Our study focuses on determining the parameter values of the excitation f, ω, and β for which the population of either species becomes dangerously low. For an example of the time evolution of the system demonstrating nonlinear effects, see Fig. 1.

For the analysis, we use the canonical AA formalism. Since Eqs. (4)–(5) do not fulfill the Hamilton equations

$$\dot{q} = \frac{\partial H}{\partial p}, \qquad \dot{p} = -\frac{\partial H}{\partial q}, \tag{8}$$

we introduce the following change of variables

$$p := -\ln x, \qquad q := -\ln\frac{y}{\Omega^2}. \tag{9}$$

Equations (4)–(5) become

$$\dot{p} = \Omega^2\left(e^{-q} - 1\right) + f\sin(\omega t + \beta), \tag{10}$$

$$\dot{q} = 1 - e^{-p},$$

$$p(0) = 0, \quad q(0) = 0. \tag{11}$$

The Hamiltonian corresponding to Eqs. (10)–(11) is given by

$$\begin{aligned} H(p,q,t) &= \underbrace{p + e^{-p} + \Omega^2\left(q + e^{-q}\right) - \Omega^2 - 1}_{=:H_0(q,p)=:\eta} \\ &\quad - q\underbrace{f\sin(\omega t + \beta)}_{=:\hat{f}(t)} \\ &= H_0(q,p) - q\hat{f}(t). \end{aligned} \tag{12}$$

Equations (10)–(11) cannot be solved exactly. Even in the case of the unperturbed Lotka-Volterra model, the explicit solution in time cannot be presented in

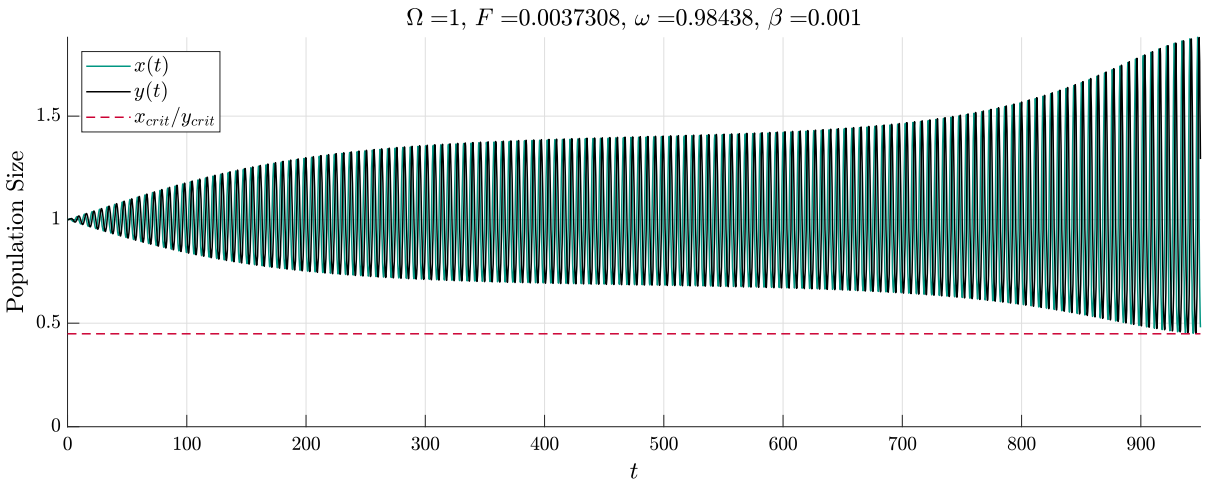

Fig. 1 Large amplitude, nonlinear vibrations caused by low-amplitude oscillations in the prey reproduction rate. Equilibrium initial conditions are used. The critical population size of both species is depicted with red dashed line. (Color figure online)

terms of known functions [12,30–32]. The exact solution to the special case with $\tilde{\alpha}_0 = -\tilde{\delta}$ was reported in [33]. However, this does not represent a true predator–prey system since the predator population can persist even if the prey population goes extinct. Until recently, no explicit analytical formula has been known for the initial-condition-dependent oscillation period in the Lotka-Volterra system [30,34]. The transformation to canonical AA coordinates in an integral form is provided in Appendix A. However, without explicit formulas, a change in the AA coordinates is unfeasible unless further simplifying assumptions are made on the model.

Therefore, we assume that the system's energy remains small, i.e., $\eta \in O(\varepsilon)$, where we use ε to denote a small but not exactly specified positive number that helps to distinguish between different orders of magnitudes. Then, we define the following non-small variables

$$E := \frac{\eta}{\varepsilon}, \quad P := \frac{p}{\sqrt{\varepsilon}}, \quad Q := \frac{q}{\sqrt{\varepsilon}}. \tag{13}$$

Further, we assume that the excitation force is small, i.e.

$$f = \varepsilon F, \quad \text{with } F \in O(1). \tag{14}$$

We also assume that the excitation frequency is close to the linearized eigenfrequency of the system, that is,

$$\omega = \Omega(1 + \sqrt{\varepsilon}\Delta), \quad \text{with } \Delta \in O(1). \tag{15}$$

Then, we expand Eqs. (10)–(11) into Taylor series, truncate the series, and neglect all terms of $o(\varepsilon)$. The surrogate model is given as

$$\dot{P} = \Omega^2 \left(-Q + \frac{\sqrt{\varepsilon} Q^2}{2} - \frac{\varepsilon Q^3}{6} \right) + \sqrt{\varepsilon} F \sin(\omega t + \beta), \tag{16}$$

$$\dot{Q} = P - \frac{\sqrt{\varepsilon} P^2}{2} + \frac{\varepsilon P^3}{6},$$
$$P(0) = 0, \quad Q(0) = 0. \tag{17}$$

Eqs. (16)–(17) remain difficult to solve analytically in closed form. Thus, we focus on the primary 1:1 resonance regime. The transient dynamics near the 1:1 resonance can be effectively analyzed using primary averaging [21,35,36]. This approach can be applied in various ways, but for generality, we employ the AA formalism. The approach is briefly presented here, based on [25]. The Hamiltonian is given as

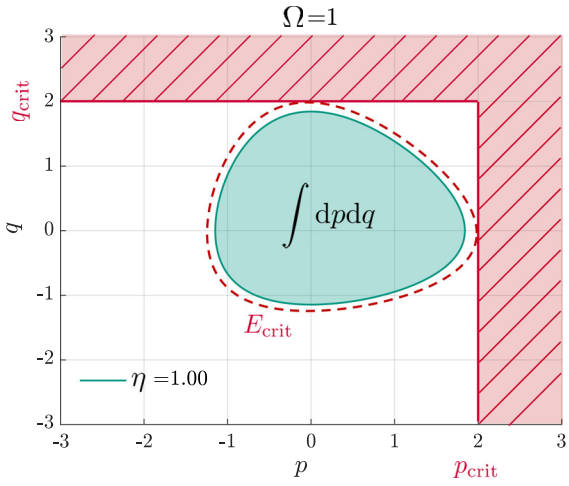

Fig. 2 Displacement vs. energy-based critical levels (shown in red). The critical upper levels of p and q depicted by continuous straight lines are in fact lower limits on x and y, as indicated by Eq. (9). The red region represents the zone where either the prey or predator species are endangered. A theoretically stricter, but practically almost equivalent boundary of the danger zone can be defined in terms of the system energy, depicted by the red dashed line. The green area enclosed by the level sets of the energy η is linearly proportional to the action $I(\eta)$. (Color figure online)

$$H_S(Q,P,t) = \underbrace{\frac{P^2}{2} - \frac{P^3}{6}\sqrt{\varepsilon} + \frac{P^4}{24}\varepsilon + \Omega^2\left(\frac{Q^2}{2} - \frac{Q^3}{6}\sqrt{\varepsilon} + \frac{Q^4}{24}\varepsilon\right)}_{:=H_0(Q,P)=E} - Q\sqrt{\varepsilon}F\sin(\omega t+\beta) \tag{18}$$

$$= H_0(Q,P) - Q\sqrt{\varepsilon}F\sin(\omega t+\beta), \tag{19}$$

where $H_0(p,q) = E$ =const. denotes the Hamiltonian of the unperturbed, surrogate autonomous system. The critical values of Q and P are given by

$$P_{\text{crit}} := -\frac{\ln(x_{\text{crit}})}{\sqrt{\varepsilon}}, \quad Q_{\text{crit}} := -\frac{\ln\left(\frac{y_{\text{crit}}}{\Omega^2}\right)}{\sqrt{\varepsilon}}. \tag{20}$$

Note that reaching both critical values at the same time, that is, $P(t_{\text{crit}}) = P_{\text{crit}}$ and $Q(t_{\text{crit}}) = Q_{\text{crit}}$ is practically impossible. We can observe that if one of the coordinates just reaches the critical level, which implies that the trajectory is tangential to the critical line, the other coordinate is close to zero (cf. Fig. 2).

Therefore, the critical energy level E_{crit} can be expressed in terms of P_{crit} and Q_{crit} as

$$E_{\text{crit}} := \min\left(\frac{P_{\text{crit}}^2}{2} - \frac{P_{\text{crit}}^3}{6}\sqrt{\varepsilon} + \frac{P_{\text{crit}}^4}{24}\varepsilon, \Omega^2\left(\frac{Q_{\text{crit}}^2}{2} - \frac{Q_{\text{crit}}^3}{6}\sqrt{\varepsilon} + \frac{Q_{\text{crit}}^4}{24}\varepsilon\right)\right). \tag{21}$$

For a graphical representation of the different level-crossing definitions, see Fig. 2.

Additionally, it is important to note that x_{crit} and y_{crit} are not only determined by P_{crit} and Q_{crit}, but also by ε. We can more conveniently redefine the level crossing condition by setting $E_{\text{crit}} := 1/2$ and choosing ε corresponding to x_{crit} and y_{crit} without significantly affecting the generality.

3 Reduction to the 1:1 resonance manifold

3.1 The general procedure

In what follows, we recapitulate the general procedure for finding a first integral of the equations averaged around the 1:1 resonance based on [25]. In general, the transformation to AA variables can be made using well-known formulas [18] for a given Hamiltonian $H_0(p,q)$:

$$I(E) = \frac{1}{2\pi}\oint P(Q,E)\mathrm{d}Q, \tag{22}$$

$$\theta(E,Q) = \frac{\partial}{\partial I}\int_0^Q P(Q,I)\mathrm{d}Q, \tag{23}$$

where $H_0(P,Q) = E$ defines a constant energy level for the unperturbed Hamiltonian $H_0(P,Q)$. By inverting expressions (22)–(23), one can then obtain explicit formulas for the canonical change of variables $P = P(I,\theta)$ and $Q = Q(I,\theta)$. Although this procedure is viable, it will be more convenient to calculate only $I(E)$ with the formula given in Eq. (22) and determine $Q(E,\theta)$ and $P(E,\theta)$ using the Linstedt-Poincaré method.

The canonical transformation defined here does not incorporate explicit time dependence; thus, the Hamiltonian of Eq. (18) is expressed in the following form in

terms of AA variables:

$$H_S = H_0(I) - Q(I,\theta)\sqrt{\varepsilon}F\sin(\omega t+\beta). \tag{24}$$

Since the conservative part of Hamiltonian (18) was used for the AA transformation, the transformed H_0 does not depend on the angle variable θ. Due to the 2π-periodicity of the angle variable, Hamiltonian (18) can be rewritten in terms of Fourier series [24,25,35]:

$$\begin{aligned} H_S =& H_0(I) - \Big(A_0^Q(I) + \sum_{n=1}^{\infty} A_n^Q(I)\cos(n\theta) \\ &+ B_n^Q(I)\sin(n\theta)\Big)\sqrt{\varepsilon}F\sin(\omega t+\beta). \end{aligned} \tag{25}$$

The Hamilton equations then become:

$$\begin{aligned} \dot{I} =& -\frac{\partial H_S}{\partial\theta} = \Bigg(\sum_{n=1}^{\infty} -A_n^Q(I)n\sin(n\theta) \\ &+ B_n^Q(I)n\cos(n\theta)\Bigg)\sqrt{\varepsilon}F\sin(\omega t+\beta), \end{aligned} \tag{26}$$

$$\begin{aligned} \dot{\theta} =& \frac{\partial H_S}{\partial I} = \frac{\partial H_0}{\partial I} - \Bigg(\frac{\partial A_0^Q(I)}{\partial I} + \sum_{n=1}^{\infty}\frac{\partial A_n^Q(I)}{\partial I}\cos(n\theta) \\ &+ \frac{\partial B_n^Q(I)}{\partial I}\sin(n\theta)\Bigg)\sqrt{\varepsilon}F\sin(\omega t+\beta). \end{aligned} \tag{27}$$

To address the 1:1 resonance regime, one should assume a slow evolution of the phase shift variable $\vartheta = \theta - \omega t - \beta$; all other phase combinations in Eqs. (26)–(27) should be treated as fast phase variables. Averaging over these fast phase variables gives the following system of slow-flow equations:

$$\dot{J} = \frac{\sqrt{\varepsilon}F}{2}\left(A_1^Q(J)\cos\Psi + B_1^Q(J)\sin\Psi\right), \tag{28}$$

$$\dot{\Psi} = \frac{\partial H_0}{\partial J} - \frac{\sqrt{\varepsilon}F}{2}\left(-\frac{\partial A_1^Q}{\partial J}\sin\Psi + \frac{\partial B_1^Q}{\partial J}\cos\Psi\right). \tag{29}$$

Here, $J(t) = \langle I(t)\rangle$ is the average of the action variable, and $\Psi(t) = \langle\vartheta(t)\rangle$ is the average of the phase difference over the fast phases. Direct differentiation shows that system (28)–(29) has the following first integral:

$$\begin{aligned} C =& H_0(J) + \frac{\sqrt{\varepsilon}F}{2}\left(A_1^Q(J)\sin\Psi - B_1^Q(J)\cos\Psi\right) \\ &- \omega J. \end{aligned} \tag{30}$$

Expression (30) defines a family of 1:1 resonance manifolds (RMs) of the system. The initial conditions determine the constant C-the values of the action and the slow phase at which the system is captured by the RM. Alternative to Eq. (30), one might formulate a conservation law with respect to the averaged energy $\xi = \langle E\rangle$ as well. In this case, the first integral reads as follows.

$$\begin{aligned} C_\xi =& \frac{\sqrt{\varepsilon}F}{2}\left(A_1^Q(J(\xi))\sin\Psi - B_1^Q(J(\xi))\cos\Psi\right) \\ &+ \xi - \omega J(\xi). \end{aligned} \tag{31}$$

3.2 Application to the Lotka-Volterra system

3.2.1 Calculation of the action

We proceed with calculating Eq. (22). It can be rewritten as a surface integral as

$$I(E) = \frac{1}{2\pi}\int_A \mathrm{d}P\mathrm{d}Q, \tag{32}$$

where A represents the area enclosed by the periodic trajectory on the $P-Q$ plane (cf. green area in Fig. 2). Suppose that the boundary of ∂A is given in polar coordinates by $R(\varphi)$, then the action becomes

$$I(E) = \frac{1}{4\pi}\int_0^{2\pi} R^2(\varphi)\mathrm{d}\varphi. \tag{33}$$

To estimate $R(\varphi)$, we use a perturbation method and assume

$$R = R_0 + \sqrt{\varepsilon}R_{1/2} + \varepsilon R_1 + \ldots \tag{34}$$

After rewriting $H_0(Q,P)$ from Eq. (18) into polar coordinates using $P = R\cos\varphi$ and $Q = R\sin\varphi$, we can insert the ansatz from Eq. (34), and solve for $R_0, R_{1/2}, \ldots$ by collecting the corresponding terms of

ε. Then, $R^2(\varphi)$ can be calculated and integrated resulting in

$$I(E) = \frac{E}{\Omega} + \frac{\Omega^2+1}{24\Omega^3}E^2\varepsilon + o(\varepsilon). \tag{35}$$

As a by-product of the calculation [18], we also obtain the energy-dependent time period as

$$T(E) = 2\pi\frac{\mathrm{d}I}{\mathrm{d}E} = \frac{2\pi}{\Omega}\left(1 + \frac{\Omega^2+1}{12\Omega^2}E\varepsilon\right) + o(\varepsilon) \tag{36}$$

Details on the calculations can be found in Appendix B.

Although not used directly in the analysis, for completeness, see Appendix C for an asymptotic analysis with large values of the energy.

3.2.2 Calculation of the angle

It is well-known [18], that the angle is a linear function of the time, more specifically

$$\theta = \frac{\mathrm{d}E}{\mathrm{d}I}t + \text{const.} \tag{37}$$

Therefore, if the trajectories of the unperturbed system $Q(t; E)$ and $P(t; E)$ can be obtained by any means, the calculation of θ as described by Eq. (23) and consecutive inversion to $Q(\theta, E)$ and $P(\theta, E)$ is no longer necessary. Obtaining such a solution is possible using the Poincaré-Linstedt method.

Suppose that the solution of Eqs. (16)–(17) with initial conditions

$$P(0) = P_*(E), \qquad Q(0) = 0, \tag{38}$$

can be written as the following series.

$$P(t) = P_0(t) + \sqrt{\varepsilon}P_{12}(t) + \varepsilon P_1(t) + \dots \tag{39}$$
$$Q(t) = Q_0(t) + \sqrt{\varepsilon}Q_{12}(t) + \varepsilon Q_1(t) + \dots \tag{40}$$

Furthermore, to be able to suppress secular terms, we reuse the letter τ to introduce the rescaled time $\tau = \Omega_\varepsilon t$ with

$$\Omega_\varepsilon = \Omega + \sqrt{\varepsilon}\omega_{12} + \varepsilon\omega_1 + \dots \tag{41}$$

Denoting the derivatives of τ by $\square'$, we can write Eqs. (16)–(17) as

$$\Omega_\varepsilon P' = \Omega^2\left(-Q + \frac{\sqrt{\varepsilon}Q^2}{2} - \frac{\varepsilon Q^3}{6}\right), \tag{42}$$

$$\begin{aligned}\Omega_\varepsilon Q' &= P - \frac{\sqrt{\varepsilon}P^2}{2} + \frac{\varepsilon P^3}{6},\\ P(0) &= P_*(E),\\ Q(0) &= 0.\end{aligned} \tag{43}$$

Details on the solution of Eqs. (42)–(43) can be found in Appendix D.

Note that τ is exactly 2π periodic, therefore $\theta \equiv \tau$. In Eq. (30), only the first Fourier coefficients of $Q(\theta, \xi)$ are needed, which are given in terms of the averaged energy as

$$A_1^Q(\xi) = -\frac{2\xi}{3\Omega^2}\sqrt{\varepsilon} - \frac{5\sqrt{2}\xi^{3/2}}{36\Omega^2}\varepsilon + \dots \tag{44}$$

$$B_1^Q(\xi) = \frac{\sqrt{2\xi}}{\Omega} - \frac{\sqrt{2}\left(7\Omega^2+11\right)\xi^{3/2}}{144\Omega^3}\varepsilon + \dots \tag{45}$$

3.3 Level-crossing mechanisms

With Eqs. (35) and (44)–(45), and taking into account the assumptions on f and ω given in Eqs. (14)–(15), the conservation law (31) can be evaluated. Omitting the terms of $o(\varepsilon)$, we find

$$\begin{aligned}C_\xi = \xi + \frac{F\sqrt{\varepsilon}}{2}\Bigg(&\left(-\frac{2\xi}{3\Omega^2}\sqrt{\varepsilon} - \frac{5\sqrt{2}\xi^{3/2}}{36\Omega^2}\varepsilon\right)\sin\Psi\\ &- \left(\frac{\sqrt{2\xi}}{\Omega} - \frac{\sqrt{2}\left(7\Omega^2+11\right)\xi^{3/2}}{144\Omega^3}\varepsilon\right)\cos\Psi\Bigg)\\ &- (1+\Delta\sqrt{\varepsilon})\xi\left(1 + \frac{\Omega^2+1}{24\Omega^2}\xi\varepsilon\right).\end{aligned} \tag{46}$$

Equation (46) can be simplified to

$$\begin{aligned}C_\xi = &-\left(\frac{F\cos(\Psi)\sqrt{2}\sqrt{\xi}}{2\Omega} + \Delta\xi\right)\sqrt{\varepsilon}\\ &-\left(\frac{F\xi\sin(\Psi)}{3\Omega^2} + \frac{\left(\Omega^2+1\right)\xi^2}{24\Omega^2}\right)\varepsilon + o(\varepsilon).\end{aligned} \tag{47}$$

Omitting terms of $o(\varepsilon)$, division by $-\sqrt{\varepsilon}$ and introducing $2N^2 := \xi$ to get rid of square roots yields a new

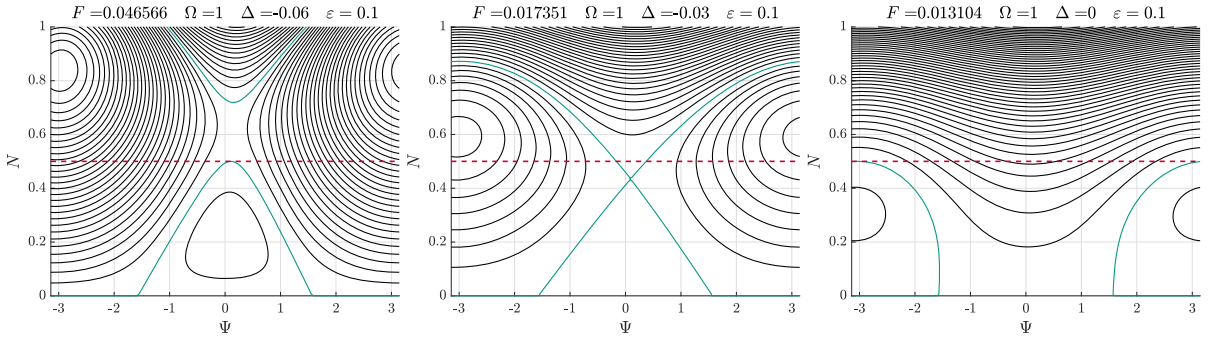

(a) Type II Maximum Mechanism (b) Saddle Mechanism (c) Type I Maximum Mechanism

Fig. 3 The levels sets of the integral of motion (48) for the three level-crossing mechanisms with critical forcing value $F_{\rm crit}$. The LPT is shown with a green continuous line. The critical level $N_{\rm crit} = 1/2$ is shown with a dashed red line. (Color figure online)

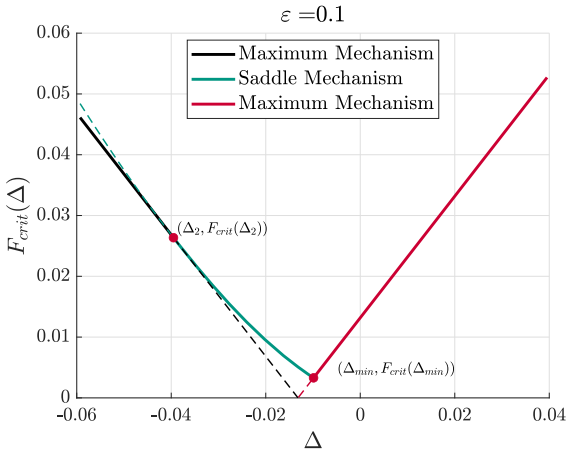

Fig. 4 Critical force amplitude $F_{\rm crit}$ depicted against the frequency deviation Δ for $\Omega = 1$ (cf. Eq. (50))

conservation law

$$D = \frac{F\cos(\Psi)\,N}{\Omega} + 2N^2\Delta + \left(\frac{2N^2 F\sin(\Psi)}{3\Omega^2} + \frac{\left(\Omega^2+1\right)N^4}{6\Omega^2}\right)\sqrt{\varepsilon}. \tag{48}$$

In contrast to the system investigated in [26], the conservation law includes the parameter ε.

Expression (48) is utilized to examine the transient dynamics on the RM further. The phase portrait on the RM aligns with the level sets of the conservation law (46). As stated in Eq. (21), the event of crossing the critical energy level $E_{\rm crit} = 1/2$ in the averaged system should correlate with the phase trajectory reaching the limit

$$N_{\rm crit} = \frac{1}{2} \tag{49}$$

for some value of the slow phase $\Psi_{\rm crit}$. Consequently, the population size of the species will reach a dangerously low level if the RM trajectory, corresponding to the chosen initial conditions, achieves $N_{\rm crit}$. As mentioned above, in this study, we focus on the trajectory with zero initial conditions, which is often also referred to as the limiting phase trajectory (LPT) [37–40]. From expression (48), it follows that the LPT is defined by the condition $D = 0$. We note that the LPT is not special to this problem, and different initial conditions would result in crossing the critical level being governed by other phase trajectories on the RM.

Two primary mechanisms for level crossing on the RM can be identified. The first mechanism, applicable to positive and small negative detuning values, as well as for large negative detuning values Δ, is illustrated in Fig. 3a and c.

In this simple scenario, for $F < F_{\rm crit}$, the LPT does not reach $N_{\rm crit}$, and the population sizes remain in the safe region. For $F > F_{\rm crit}$, the LPT reaches $N_{\rm crit}$, resulting in critical population sizes. At the boundary $F = F_{\rm crit}$, the line $N = N_{\rm crit}$ is tangent to the LPT at some $\Psi_{\rm crit}$ (cf. Fig. 3a and c). We will refer to this level-crossing scenario as the maximum mechanism.

For larger negative detuning values, crossing the critical level occurs through a more complex scenario, as shown in Fig. 3b. In this scenario, for $F < F_{\rm crit}$, the LPT stays below the saddle point on the RM, and the population size remains in the safe zones.

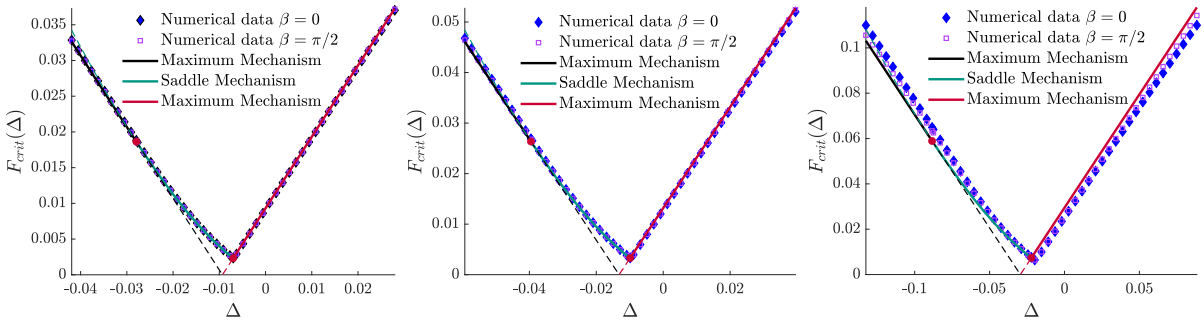

(a) $\varepsilon = 0.05$ (b) $\varepsilon = 0.1$ (c) $\varepsilon = 0.5$

Fig. 5 Comparison of the analytical model with simulation results generated by the surrogate Lotka-Volterra model given by Eqs. (16)–(17). For simulations, three different values of ε are used. Two different initial phase values $\{0, \pi\}$ are applied in each case. At time $t = 0$, the system is in (non-trivial) equilibrium. $\Omega = 1$

For $F > F_{\text{crit}}$, the level crossing occurs. The threshold $F = F_{\text{crit}}$ signifies the point at which the LPT reaches the saddle (over an infinite amount of time). An infinitesimal increment of F causes the LPT to approach the saddle infinitely closely. However, instead of reaching it, the solution's amplitude starts to grow-initially gradually, then increasingly rapidly-eventually reaching the critical level (cf. Fig. 1). This process is known as the saddle mechanism.

It is worth emphasizing that the level-crossing problem of the Lotka-Volterra system with small nonlinearities (cf. Eqs. (16)–(17)) is primarily governed by the maximum mechanism, with the saddle mechanism emerging due to nonlinear perturbations. Even small nonlinearities lead to significant changes in the system dynamics. Due to the simplicity of the integral of motion (48), explicit expressions can be derived for the critical forcing depending on the frequency detuning for both transition scenarios. The critical forcing curve is given by

$$F_{\text{crit}}(\Delta) \approx \begin{cases} -\Delta\Omega - \frac{\Omega^2+1}{48\Omega}\sqrt{\varepsilon} & \text{for } \Delta < \Delta_2, \\ \frac{8\Omega^2(-\Delta)^{\frac{3}{2}}}{3\sqrt{\Omega^2+1}}\varepsilon^{-\frac{1}{4}} & \text{for } \Delta_2 < \Delta < \Delta_{\min}, \\ \Delta\Omega + \frac{\Omega^2+1}{48\Omega}\sqrt{\varepsilon} & \text{for } \Delta_{\min} < \Delta, \end{cases} \tag{50}$$

with the interval boundaries

$$\Delta_{\min} \approx -\frac{(\Omega^2+1)}{64\Omega^2}\sqrt{\varepsilon}, \quad \Delta_2 \approx -\frac{(\Omega^2+1)}{16\Omega^2}\sqrt{\varepsilon}. \tag{51}$$

The minimally needed force amplitude is given at the intersection of the saddle and the right branch of the maximum mechanism at $\Delta_{\text{crit,min}}$ as

$$F_{\text{crit,min}} \approx \frac{(\Omega^2+1)}{192\Omega}\sqrt{\varepsilon} \tag{52}$$

For the detailed derivation of the critical forcing curve, see Appendix E. For $\varepsilon = 0.1$, the critical force is shown in Fig. 4. The results show qualitative similarity to those found in [26], with the difference that the bookkeeping parameter ε remains in the expression.

4 Numerical results and model validation

This section presents the numerical results and validates the model using various analyses. First, we perform an analysis using the surrogate model given in Eqs. (16)–(17) with $\Omega = 1$, $\varepsilon = \{0.05, 0.1, 0.5\}$ and for the initial phase excitation values of $\beta = \{0, \pi/2\}$. The results are depicted in Fig. 5, illustrating the critical force curves $F_{\text{crit}}(\Delta)$.

In Fig. 6, the same analysis is performed, but with the original model, given in Eqs. (10)–(11), for the same initial phase values but with $\Omega = 2$.

The results indicate a good agreement between the analytical and numerical models for smaller values of ε, and even for $\varepsilon = 0.5$, the agreement remains reasonably good. The analytical model can predict significant variations in the system, potentially reducing the population size by half (cf. Fig. 1), which is a substantial

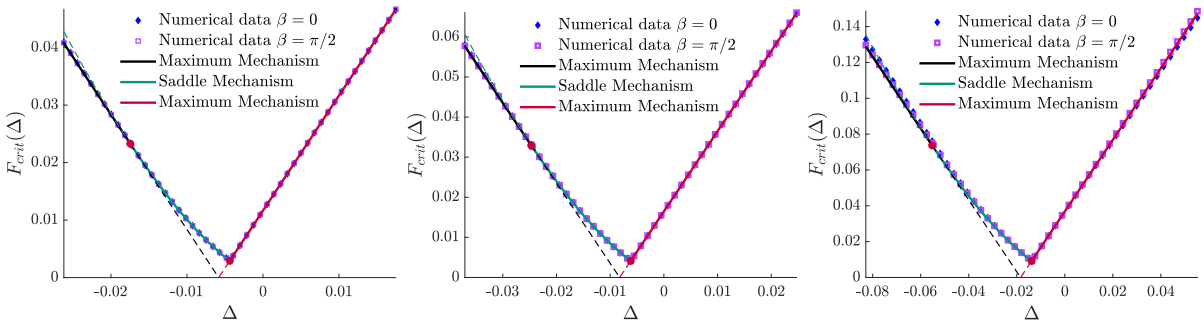

Fig. 6 Comparison of the analytical model with simulation results generated by the original Lotka-Volterra model given by Eqs. (4)–(5). For simulations, three different values of ε are used. Two different initial phase values $\{0, \pi\}$ are applied in each case. At time $t = 0$, the system is in (non-trivial) equilibrium. $\Omega = 2$

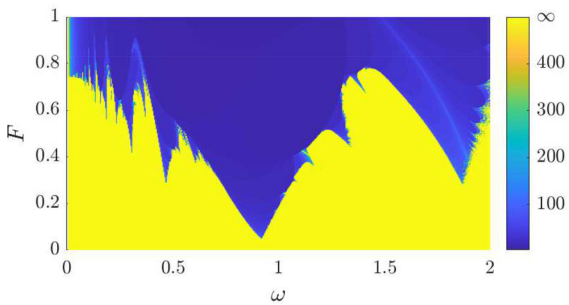

Fig. 7 Level-crossing time of the Lotka-Volterra model with periodic variations depicted against the excitation frequency ω and excitation amplitude F for initial phase $\beta = \pi/2$, $\Omega = 1$ and equilibrium initial conditions. The critical population size is taken to be 10% of the equilibrium population size. The simulations are integrated up to $t_{\text{end}} = 500$

impact. We can observe that in the vicinity of the minimum critical force $F_{\text{crit,min}}$, the effect of the excitation's initial phase, as predicted by the analytical model, is negligible.

Finally, in Fig. 7, numerical simulation results of the level-crossing time of the original Lotka-Volterra model depicted against the excitation frequency and amplitude are shown with $\Omega = 1$ for a critical population size $x_{\text{crit}} = y_{\text{crit}} = 0.1$. Strong nonlinear effects can be observed further away from the minimum, such as fractal-like boundary and sub- and superharmonic resonances. However, even in the strongly nonlinear system, no chaos is observed around the sharp V-shaped minimum at these levels of the critical population sizes.

5 Conclusions and scope for future research

In this study, we examined the effects of seasonal variations on the reproductive rates of prey species. These variations can result from various factors such as hunting, temporal variations in food availability, disease, or other causes that lead to population oscillations. Our findings indicate that significant amplitude variations can arise when the system is initiated at equilibrium. These variations have a dual impact: they can jeopardize the population by driving it to critically low levels, but they also offer potential control mechanisms. For example, regulated hunting could mitigate these variations, thereby reducing excitation within the system.

The implications of these results extend to integrated farming models where predator and prey species are co-farmed. Strategic harvesting of one or both species can optimize farm yield in such systems. Additionally, our research demonstrates that converting to AA variables and subsequent averaging around the principal resonant manifold traditionally applied to naturally Hamiltonian systems, such as mechanical ones being quadratic in momenta, can be effectively applied to any Hamiltonian system. Specifically, we have shown that this approach applies to the Lotka-Volterra model, a non-naturally Hamiltonian system.

Our analysis revealed a pronounced minimum in the critical forcing amplitude when initial conditions commence at equilibrium, reflecting results observed in the previous literature. Looking ahead, several new research directions emerge from our findings. A nat-

ural extension is to analyze the dynamical integrity of the Lotka-Volterra system by incorporating non-equilibrium initial conditions, which involves studying the safe basins of the dynamics and sensitivity to excitation amplitude and frequency [41].

Based on Fig. 7, it may be worthwhile to investigate the 2:1 resonance within the same model. A similar V-shaped curve appears around an excitation frequency that is twice the frequency of the main resonance, investigated in the current paper.

Furthermore, the hybrid approach to transitioning from the original coordinates to the action and angle coordinates, where the angle variable is treated as a stretched time, offers a new perspective. This method is suitable for small perturbations using the Linstedt-Poincaré method and may also work for larger nonlinearities if the exact solution of the basic Hamiltonian can still be computed, allowing for an extension of the method for other Hamiltonian systems (e.g., epidemology [42,43]). These systems, characterized by conservation laws that can be interpretable as energy, can benefit from the analysis performed here.

In conclusion, our research provides a framework for understanding and controlling population variations in predator–prey systems and offers insights for broader applications across various scientific disciplines dealing with ordinary differential equations.

Acknowledgements We acknowledge the assistance of AI tools, including OpenAI's ChatGPT (version GPT-4o), Grammarly, and Writefull, for language editing and refinement in preparing this article.

Funding Open Access funding enabled and organized by Projekt DEAL. This research was funded by the Deutsche Forschungsgemeinschaft (DFG, German Research Foundation) under Project Number 508244284. We are sincerely grateful for their support. The results presented in this paper were achieved during a research stay in Ancona. This stay was generously funded by the Karlsruhe House of Young Scientists (KHYS), for which we are deeply grateful.

Data Availability Statement This manuscript has no associated data.

Declarations

Conflict of interest The authors declare that they have no conflict of interest.

Appendices

Appendix A: Conversion to AA coordinates of the strongly-nonlinear LV system

We start with the Hamiltonian given by

$$H(q,p) = p + e^{-p} + \Omega^2\left(q + e^{-q}\right) - \alpha - 1 = \eta. \tag{53}$$

By isolating p, we have:

$$p + e^{-p} = \eta + \Omega^2 + 1 - \Omega^2\left(q + e^{-q}\right) =: z(\eta, q). \tag{54}$$

To solve this equation, we transform it into the standard form for the Lambert W function. Let $x = -e^{-p}$. Then, we have:

$$xe^{x} = -e^{-z}. \tag{55}$$

The Lambert W function gives the solution to this equation [44]:

$$x = W_n\left(-e^{-z}\right). \tag{56}$$

Substituting back for x, we obtain:

$$p = -\ln(-x) = \ln\left(\frac{1}{-W_n\left(-e^{-z}\right)}\right). \tag{57}$$

Alternatively, we can express p directly in terms of the Lambert W function [44]:

$$p = W_n\left(-e^{-z}\right) + z. \tag{58}$$

In our specific case, z is real. Hence, the branches W_{-1} and W_0 of the Lambert W function are sufficient to describe our solutions corresponding to $p_-(q)$ and $p_+(q)$, respectively (cf. Fig. 8).

We define

$$\mu := \frac{\eta}{\Omega^2} + 1. \tag{59}$$

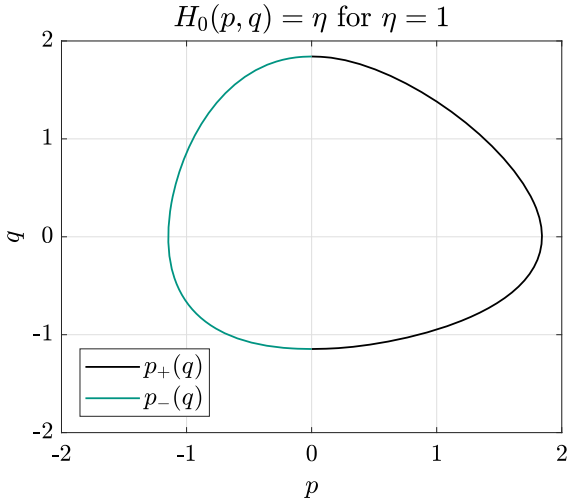

Fig. 8 The functions $p_-(q)$ and $p_+(q)$

The extremal values of q are given by:

$$q_{\min} = W_{-1}\left(-e^{-\mu}\right) + \mu, \tag{60}$$

$$q_{\max} = W_0\left(-e^{-\mu}\right) + \mu. \tag{61}$$

The action $I(\eta)$ can be written as:

$$I(\eta) = \frac{1}{2\pi}\oint p(q,\eta)dq \tag{62}$$

$$= \frac{1}{2\pi}\int_{q_{\min}}^{q_{\max}} \left(p_+(q,\eta) - p_-(q,\eta)\right) dq. \tag{63}$$

Substituting the expressions for p_+ and p_-:

$$I(\eta) = \frac{1}{2\pi}\int_{q_{\min}}^{q_{\max}} W_0\left(-e^{-z}\right) - W_{-1}\left(-e^{-z}\right) dq. \tag{64}$$

Similarly, the angle variable θ is given by:

$$\theta(q,\eta) = \frac{d\eta}{dI}\int_0^q \frac{\partial p(q,\eta)}{\partial \eta} dq. \tag{65}$$

With the expression for p:

$$\theta(q,\eta) = \frac{d\eta}{dI}\int_0^q \frac{1}{1 + W_n\left(-e^{-z}\right)} dq. \tag{66}$$

Despite these manipulations, no analytical solution could be found for these integrals. Finding the integrals would be equivalent to finding the explicit analytical solution of the Lotka-Volterra equations. The closest attempt in the literature with $\Omega = 1$ can be found in [31].

Appendix B: Calculation of the action for small energy values

We start by rewriting the Hamiltonian of the unperturbed surrogate problem given by H_0 in polar coordinates by inserting $P = R\cos\varphi$ and $Q = R\sin\varphi$:

$$H_0(Q,P) = \frac{R^2\cos^2\varphi}{2} - \sqrt{\varepsilon}\frac{R^3\cos^3\varphi}{6} + \varepsilon\frac{R^4\cos^4\varphi}{24} + \Omega^2\left(\frac{R^2\sin^2\varphi}{2} - \sqrt{\varepsilon}\frac{R^3\cos^3\varphi}{6} + \varepsilon\frac{R^4\cos^4\varphi}{24}\right) = E. \tag{67}$$

We define:

$$A(\varphi) := \frac{\cos^4\varphi + \alpha\sin^4\varphi}{24}, \tag{68}$$

$$B(\varphi) := \frac{\cos^3\varphi + \alpha\sin^3\varphi}{6}, \tag{69}$$

$$C(\varphi) := \frac{\cos^2\varphi + \alpha\sin^2\varphi}{2} \tag{70}$$

Thus, we have:

$$A(\varphi)R^4\varepsilon - B(\varphi)R^3\sqrt{\varepsilon} + C(\varphi)R^2 = E. \tag{71}$$

Assuming $R = R_0 + \sqrt{\varepsilon}R_{1/2} + \varepsilon R_1 + \ldots$, we substitute in Eq. (71) and collect the terms of ε^0, $\varepsilon^{1/2}$, ε resulting in

$$\begin{aligned} &CR_0^2 \quad -E \\ &\quad +(2CR_{1/2}R_0 - BR_0^3)\sqrt{\varepsilon} \\ &\quad +(AR_0^4 - 3BR_{1/2}R_0^2 + CR_{1/2}^2 + 2CR_0R_1)\varepsilon + \ldots \\ &\quad = 0. \end{aligned} \tag{72}$$

Solving for R_0, $R_{1/2}$, R_1, we find:

$$R_0 = \frac{\sqrt{E}}{\sqrt{C}}, \quad R_{1/2} = \frac{BE}{2C^2}, \quad R_1 = \frac{5B^2 - 4AC}{8C^{7/2}}E^{3/2}. \tag{73}$$

Thus, the radius R and its square R^2 are given by:

$$R = \frac{\sqrt{E}}{\sqrt{C}} + \frac{B}{2C^2}E\sqrt{\varepsilon} + \frac{5B^2 - 4AC}{8C^{7/2}}E^{3/2}\varepsilon + O(\varepsilon^{3/2}), \tag{74}$$

$$R^2 = \frac{E}{C} + \frac{BE^{3/2}}{C^{5/2}}\sqrt{\varepsilon} + \left(\frac{B^2}{4C^4} + \frac{5B^2 - 4AC}{4C^4}\right)E^2\varepsilon$$

$$+ O(\varepsilon^{3/2}). \tag{75}$$

The action becomes:

$$\begin{aligned} I(E) &= \frac{1}{2\pi}\int_0^{2\pi}\frac{R^2(\varphi)}{2}\,d\varphi \\ &= \frac{1}{4\pi}\int_0^{2\pi}\left(\frac{E}{C}+\frac{BE^{3/2}}{C^{5/2}}\sqrt{\varepsilon}\right. \\ &\quad \left.+\left(\frac{B^2}{4C^4}+\frac{5B^2-4AC}{4C^4}\right)E^2\varepsilon\right)\mathrm{d}\varphi+O(\varepsilon^{3/2}) \end{aligned} \tag{76}$$

$$\begin{aligned} I(E) &= \frac{E}{\Omega}+\frac{\Omega^2+1}{24\Omega^3}E^2\varepsilon \\ &\quad + o(\varepsilon). \end{aligned} \tag{77}$$

Finally, the period T is given by:

$$T = 2\pi\frac{\mathrm{d}I}{\mathrm{d}E} = \frac{2\pi}{\Omega}\left(1+\frac{\Omega^2+1}{12\Omega^2}E\varepsilon\right)+o(\varepsilon). \tag{78}$$

Appendix C: Calculation of the action for large energy values

In Appendix A, the action was given as an integral, but its explicit value remained unknown since we were unable to evaluate the integral in a closed form. In Appendix B, we determined the action for small energy values. Now, we analyze the case where the energy is large, i.e. $H_0(p,q) = \eta \gg 1$, allowing for some assumptions about the function $H_0(p,q)$. Since $I = \text{Area}/2\pi$, we focus on finding the area enclosed by the curve defined by $H_0(p,q) = \eta$. We define the total area into three different sections as shown in Fig. 9

We approximate the three parts one by one under different assumptions:

- A_1: $q \gg e^{-q}$,
- A_2: $p \gg e^{-p}$,
- A_3: $q \ll e^{-q}$ and $p \ll e^{-p}$.

Under these assumptions, $H_0(p,q) = \eta$ can be simplified to the following equations.

$$q_1(p) \approx \frac{\eta+1+\Omega^2-p-e^{-p}}{\Omega^2}, \tag{79}$$

$$p_2(q) \approx \eta+1+\Omega^2-\Omega^2\left(q+e^{-q}\right), \tag{80}$$

$$q_3(p) \approx -\ln\left(\eta+1+\Omega^2-e^{-p}\right)+2\ln\Omega. \tag{81}$$

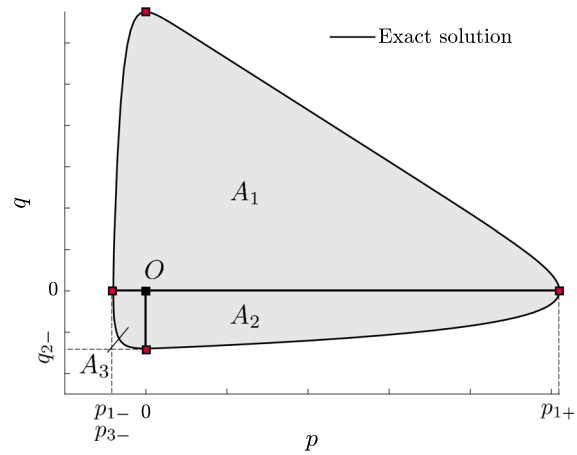

Fig. 9 Dividing the area enclosed by the unperturbed Hamiltonian $H_0(p,q)$ into different parts

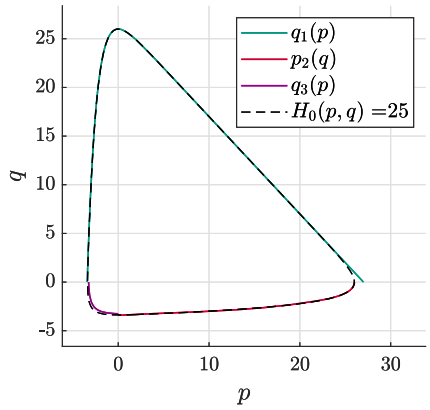

Fig. 10 Surrogate boundaries for $H_0(p,q) = \eta = 25$ and $\Omega = 1$

p_1^-, p_1^+, q_2^- and p_3^- denote the positive and negative roots of each equations, respectively. Equations (79)–(81) are depicted in Fig. 10 for $\eta = 25$ and $\Omega = 1$.

The areas are given by the integrals:

$$\begin{aligned} A_1 &= \int_{p_1^-}^{p_1^+} q_1(p)\,\mathrm{d}p, \quad A_2 = \int_{q_2^-}^{0} p_2(q)\,\mathrm{d}q, \\ A_3 &= -\int_{p_3^-}^{0} q_3(p)\,\mathrm{d}p, \end{aligned} \tag{82}$$

where:

$$p_1^- := W_{-1}\left(-e^{-\eta-\Omega^2-1}\right)+\eta+\Omega^2+1, \tag{83}$$

$$p_1^+ := W_0\left(-e^{-\eta-\Omega^2-1}\right)+\eta+\Omega^2+1, \tag{84}$$

$$q_2^- := W_{-1}\left(-e^{-\frac{\eta+\Omega^2+1}{\Omega^2}}\right) + \frac{\eta+\Omega^2+1}{\Omega^2}, \tag{85}$$

$$p_3^- := -\ln(\eta+1). \tag{86}$$

The areas become

$$A_1 = \left[\frac{\eta+1+\Omega^2}{\Omega^2}p - \frac{p^2}{2\Omega^2} + \frac{e^{-p}}{\Omega^2}\right]_{p_1^-}^{p_1^+}, \tag{87}$$

$$A_2 = \left[(\eta+1+\Omega^2)q - \Omega^2\left(\frac{q^2}{2} - e^{-q}\right)\right]_{q_2^-}^{0}, \tag{88}$$

$$A_3 = \left[\mathrm{Li}_2\left(\frac{e^{-p}}{\eta+1+\Omega^2}\right) + p\ln\frac{\eta+1+\Omega^2}{\Omega^2}\right]_{p_3^-}^{0}. \tag{89}$$

where $\mathrm{Li}_n(x)$ denotes the dilogarithm, defined as

$$\mathrm{Li}_2(z) := -\int_0^z \frac{\ln(1-t)}{t}\,\mathrm{d}t. \tag{90}$$

After the insertion of the integral boundaries and subsequent simplifications, the areas become:

$$A_1(\eta) = \frac{1}{2\Omega^2}\Big(W_{-1}^2(-e^{-B}) + 2W_{-1}(-e^{-B}) - W_0^2(-e^{-B}) - 2W_0(-e^{-B})\Big), \tag{91}$$

$$A_2(\eta) = \Omega^2\left(1 - \frac{C^2}{2} + \frac{W_{-1}^2(-e^{-C})}{2} + W_{-1}(-e^{-C})\right), \tag{92}$$

$$A_3(\eta) = \mathrm{Li}_2\left(\frac{1}{\eta+1+\Omega^2}\right) - \mathrm{Li}_2\left(\frac{\eta+1}{\eta+1+\Omega^2}\right) + \ln(\eta+1)\ln\frac{\eta+1+\Omega^2}{\Omega^2}, \tag{93}$$

with

$$B := \eta + \Omega^2 + 1, \qquad C := \frac{\eta+\Omega^2+1}{\Omega^2}. \tag{94}$$

The time period is given by:

$$T = \frac{\mathrm{d}A}{\mathrm{d}\eta} = \frac{\mathrm{d}(A_1+A_2+A_3)}{\mathrm{d}\eta}. \tag{95}$$

After differentiation and simplification, we get:

$$\frac{\mathrm{d}A_1}{\mathrm{d}\eta} = \frac{W_0\left(-e^{-\eta-1-\Omega^2}\right) - W_{-1}\left(-e^{-\eta-1-\Omega^2}\right)}{\Omega^2}, \tag{96}$$

$$\frac{\mathrm{d}A_2}{\mathrm{d}\eta} = -\frac{\eta+1+\Omega^2+\Omega^2 W_{-1}\left(-e^{-\frac{\eta+1+\Omega^2}{\Omega^2}}\right)}{\Omega^2}, \tag{97}$$

$$\frac{\mathrm{d}A_3}{\mathrm{d}\eta} = \frac{\ln\left(\frac{(\eta+1)\eta}{\Omega^2}+\eta+1\right)}{\eta+\Omega^2+1}. \tag{98}$$

Assuming large values of η, we can focus on the asymptotic behavior by taking only the leading-order terms [45]:

$$\frac{\mathrm{d}A_1}{\mathrm{d}\eta} = \frac{\eta}{\Omega^2} + \frac{\ln(\eta+1+\Omega^2)}{\Omega^2} + \frac{1+\Omega^2}{\Omega^2} + O\left(\frac{\ln\eta}{\eta}\right), \tag{99}$$

$$\frac{\mathrm{d}A_2}{\mathrm{d}\eta} = \frac{\ln\left(\eta+1+\Omega^2\right)}{\Omega^2} - \frac{2\ln\Omega}{\Omega^2} + O\left(\frac{\ln\eta}{\eta}\right), \tag{100}$$

$$\frac{\mathrm{d}A_3}{\mathrm{d}\eta} = O\left(\frac{\ln\eta}{\eta}\right). \tag{101}$$

In total, for the asymptote, we have:

$$T_A \approx \frac{\eta}{\Omega^2} + \frac{2}{\Omega^2}\ln(\eta+1+\Omega^2) + 1 + \frac{1}{\Omega^2} - 2\frac{\ln\Omega}{\Omega^2} + O\left(\frac{\ln\eta}{\eta}\right), \tag{102}$$

which differs in the leading-order term from the time period obtained for small values of the energy being η/Ω.

Figures 11 and 12 compare the exact time periods found numerically with the analytical estimates for small η (cf. Equation (78)), for large η (cf. Equation (95)), and for the asymptotic expansion of Eq. (95) given by Eq. (102), with two different values for $\Omega = \{1, 2\}$. We can see a good agreement with the exact numerical data for η values where the assumptions of the calculations are met, respectively. In the particular case of $\Omega = 1$, the estimate for small η remains valid even for large values of η.

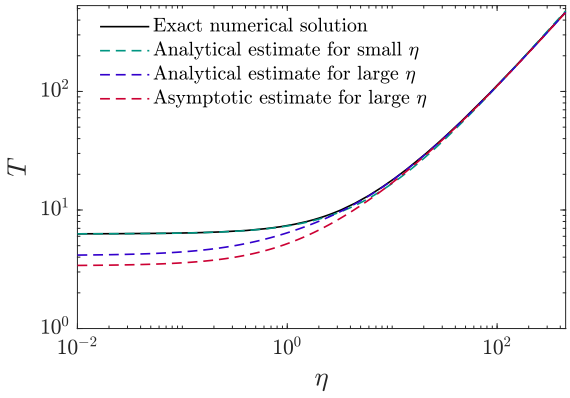

Fig. 11 Log-log plot of the time period of the solution depicted against the energy η for $\Omega = 1$. In this special case, the analytic estimate for small energy values (cf. Equation (78)) also works well even if η is large

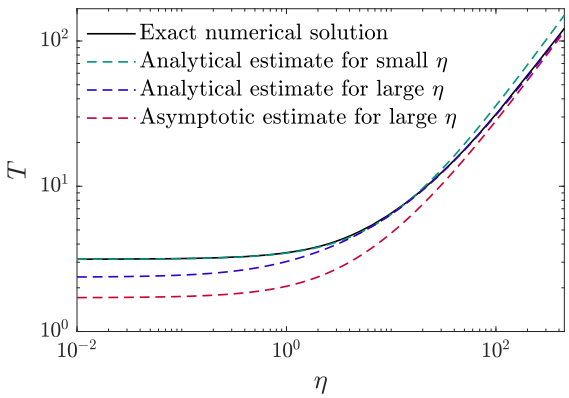

Fig. 12 Log-log plot of the time period of the solution depicted against the energy η for $\Omega = 2$. The analytic estimate for small energy values (cf. Equation (78)) does not work for large η values

Appendix D: Solution of the unperturbed system with the Poincaré-Linstedt method

Based on Eqs. (16)–(17), the unperturbed system is given by

$$\dot{P} \approx \Omega^2 \left(-Q + \frac{\sqrt{\varepsilon} Q^2}{2} - \frac{\varepsilon Q^3}{6} \right), \tag{103}$$

$$\dot{Q} \approx P - \frac{\sqrt{\varepsilon} P^2}{2} + \frac{\varepsilon P^3}{6}, \tag{104}$$

We apply the Poincaré-Lindstedt method, assuming:

$$\Omega_\varepsilon = \Omega + \sqrt{\varepsilon}\omega_{1/2} + \varepsilon\omega_1 + \ldots, \tag{105}$$

$$P(t) = P_0(t) + \sqrt{\varepsilon} P_{1/2}(t) + \varepsilon P_1(t) + \ldots, \tag{106}$$

$$Q(t) = Q_0(t) + \sqrt{\varepsilon} Q_{1/2}(t) + \varepsilon Q_1(t) + \ldots. \tag{107}$$

Inserting these expansions into the equations, we collect the terms of different orders of magnitudes:

$$\varepsilon^0 : \quad P_0' = -\Omega Q_0, \quad Q_0' = \frac{1}{\Omega} P_0, \tag{108}$$

$$\varepsilon^{1/2} : \quad P_{1/2}' = -\Omega Q_{1/2} - \frac{\omega_{1/2}}{\Omega} P_0' + \frac{\Omega}{2} Q_0^2, \tag{109}$$

$$Q_{1/2}' = \frac{1}{\Omega} P_{1/2} - \frac{\omega_{1/2}}{\Omega} Q_0' - \frac{P_0^2}{2\Omega}, \tag{110}$$

$$\varepsilon^1 : \quad P_1' = -\Omega Q_1 - \frac{\omega_{1/2}}{\Omega} P_{1/2}' - \frac{\omega_1}{\Omega} P_0' + \Omega Q_0 Q_{1/2} - \frac{\Omega Q_0^3}{6}, \tag{111}$$

$$Q_1' = \frac{1}{\Omega} P_1 - \frac{\omega_{1/2}}{\Omega} Q_{1/2}' - \frac{\omega_1}{\Omega} Q_0' - \frac{Q_0 Q_{1/2}}{\Omega} + \frac{Q_0^3}{6\Omega}. \tag{112}$$

The initial conditions are:

$$\begin{aligned} P_0(0) &= P_*(E), & Q_0(0) &= 0, \\ P_{1/2}(0) &= 0, & Q_{1/2}(0) &= 0, \\ P_1(0) &= 0, & Q_1(0) &= 0. \end{aligned}$$

The leading order system with ε^0 has the solution:

$$P_0(\tau) = P_* \cos(\tau), \quad Q_0(\tau) = \frac{P_*}{\Omega} \sin(\tau). \tag{113}$$

Thus, we have the following inhomogeneous linear ODES for $\varepsilon^{1/2}$.

$$P_{12}' = -\Omega Q_{12} + \frac{P_* \omega_{12} \sin\tau}{\Omega} + \frac{P_*^2 \sin^2\tau}{2\Omega} \tag{114}$$

$$Q_{12}' = \frac{1}{\Omega} P_{12} - \frac{P_* \cos\tau \omega_{12}}{\Omega^2} - \frac{P_*^2 \cos^2\tau}{2\Omega}. \tag{115}$$

We set $\omega_{1/2} = 0$ to suppress secular terms.

Continuing in this manner, we find solutions for $P_{1/2}(\tau)$, $Q_{1/2}(\tau)$, $P_1(\tau)$, and $Q_1(\tau)$, eventually leading to the expression for ω_1:

$$\omega_1 := -\frac{P_*^2(\Omega^2 + 1)}{24\Omega}, \tag{116}$$

in order to suppress further secular terms. Finally, combining all orders and noting that the solution in τ is

periodic in 2π, i.e., $\theta \equiv \tau$, the solution in terms of Fourier series of the angle is obtained as

$$P(E,\theta) = A_0^P + \sum_{n=1}^{\infty}\left(A_n^P \cos(n\theta) + B_n^P \sin(n\theta)\right), \tag{117}$$

$$Q(E,\theta) = A_0^Q + \sum_{n=1}^{\infty}\left(A_n^Q \cos(n\theta) + B_n^Q \sin(n\theta)\right). \tag{118}$$

We truncate the expansion at $n = 3$, as any further terms have only a contribution of $o(\varepsilon)$.

$$\begin{aligned}
P(P_*(E),\theta) = {} & \frac{P_*^2(-\varepsilon P_* + 3\sqrt{\varepsilon})}{12} - \frac{P_*(-13\Omega^2 P_*^2\varepsilon + 48\sqrt{\varepsilon}\Omega^2 P_* + 23\varepsilon P_*^2 - 288\Omega^2)}{288\Omega^2}\cos(\theta) \\
& + \frac{P_*^2(-3\varepsilon P_* + 8\sqrt{\varepsilon})}{24\Omega}\sin(\theta)\frac{P_*^2(-\Omega^2 P_*\varepsilon + 3\sqrt{\varepsilon}\Omega^2 - 4\varepsilon P_*)}{36\Omega^2}\cos(2\theta) \\
& - \frac{P_*^2\sqrt{\varepsilon}}{6\Omega}\sin(2\theta) + \frac{P_*^3\varepsilon(\Omega^2-3)}{96\Omega^2}\cos(3\theta) + \frac{P_*^3\varepsilon}{24\Omega}\sin(3\theta) + o(\varepsilon),
\end{aligned} \tag{119}$$

$$\begin{aligned}
Q(P_*(E),\theta) = {} & \frac{1}{12}\frac{P_*^2}{\Omega^2}(-\varepsilon P_* + 3\varepsilon^{1/2}) \\
& - \frac{1}{24}\frac{P_*^2}{\Omega^2}(-\varepsilon P_* + 8\varepsilon^{1/2})\cos(\theta) \\
& - \frac{1}{288}\frac{P_*(-\Omega^2 P_*^2\varepsilon + 48\varepsilon^{1/2}\Omega^2 P_* + 11\varepsilon P_*^2 - 288\Omega^2)}{\Omega^3}\sin(\theta) \\
& + \frac{1}{12}\frac{P_*^2}{\Omega^2}(\varepsilon P_* + \varepsilon^{1/2})\cos(2\theta) \\
& - \frac{1}{18}\frac{P_*^2(-\Omega^2 P_*\varepsilon + 3\varepsilon^{1/2}\Omega^2 - \varepsilon P_*)}{\Omega^3}\sin(2\theta) \\
& - \frac{1}{24}\frac{P_*^3}{\Omega^2}\varepsilon\cos(3\theta) \\
& + \frac{1}{96}\frac{P_*^3\varepsilon(3\Omega^2-1)}{\Omega^3}\sin(3\theta).
\end{aligned} \tag{120}$$

Assuming 1:1 resonance in Eqs. (26)–(27), the relevant coefficients are only $A_1^Q(E)$ and $B_1^Q(E)$. From

$$\frac{P_*^2}{2} - \sqrt{\varepsilon}\frac{P_*^3}{6} + \varepsilon\frac{P_*^4}{24} = E, \tag{121}$$

we can express P_* as follows.

$$P_* \approx \sqrt{2E} + \frac{E}{3}\sqrt{\varepsilon} + \frac{\sqrt{2}E^{3/2}}{18}\varepsilon + o(\varepsilon), \tag{122}$$

which yields

$$A_1^Q(E) = -\frac{2E}{3\Omega^2}\sqrt{\varepsilon} - \frac{5\sqrt{2}E^{3/2}}{36\Omega^2}\varepsilon + \ldots \tag{123}$$

$$B_1^Q(E) = \frac{\sqrt{2E}}{\Omega} - \frac{\sqrt{2}\left(7\Omega^2+11\right)E^{3/2}}{144\Omega^3}\varepsilon + \ldots \tag{124}$$

Appendix E: Obtaining the critical force curve

E.1 Maximum mechanism

In the case of the maximum mechanism, the maximum value of N along its trajectory reaches a predefined threshold $N_{\max} = 1/2$ at its maximum. Since $N(\Psi)$ is smooth at the maximum, the curve is tangent to the critical level line $N_{\max}$. Since we focus on the initial equilibrium conditions, we also know the value of the first integral at the maximum: $D = 0$. To find the critical force using the maximum mechanism, we start by solving the following equation.

$$\left.\frac{\partial N}{\partial \Psi}\right|_{\Psi_{1,2}} = \left.\frac{\partial D}{\partial \Psi}\right|_{\Psi_{1,2}(N)} = 0. \tag{125}$$

Next, we solve:

$$\left.D(N_{\max}, \Psi_{1,2}(N_{\max}); F_{\text{crit}})\right|_{N_{\max}=\frac{1}{2}} = 0, \tag{126}$$

which yields the critical force $F_{\text{crit,MM}}(\Delta, \Omega, \varepsilon)$. From condition $\frac{\partial D}{\partial \Psi} = 0$, we get:

$$2FN^2\cos(\Psi)\sqrt{\varepsilon} - \frac{F\sin(\Psi)N}{\Omega} = 0 \tag{127}$$

Solving for $\Psi_{1,2}$:

$$\Psi_{1,2} = \begin{cases} \arctan\left(\frac{2N\sqrt{\varepsilon}}{3\Omega}\right), \\ \arctan\left(\frac{2N\sqrt{\varepsilon}}{3\Omega}\right) + \pi. \end{cases} \tag{128}$$

Inserting $N_{\max} = \frac{1}{2}$ into $D(N_{\max}, \Psi_{1,2}) = 0$, we find:

$$F_{\text{crit,MM,1,2}} = \pm\frac{48\Delta\Omega^2 + \sqrt{\varepsilon}(\Omega^2+1)}{16\sqrt{9\Omega^2+\varepsilon}} \tag{129}$$

$$\approx \begin{cases} -\Delta\Omega - \frac{\Omega^2+1}{48\Omega}\sqrt{\varepsilon} + O(\varepsilon) \\ \Delta\Omega + \frac{\Omega^2+1}{48\Omega}\sqrt{\varepsilon} + O(\varepsilon) \end{cases} \tag{130}$$

E.2 Saddle mechanism

The saddle mechanism is more intricate than the maximum mechanism. We have to solve the three equations to find the critical force in this case. Since $D(N, \Psi)$ is smooth, the saddle must fulfill

$$\left.\frac{\partial D}{\partial \Psi}\right|_{N_{\text{saddle}},\Psi_{\text{saddle}}} = 0, \tag{131}$$

$$\left.\frac{\partial D}{\partial N}\right|_{N_{\text{saddle}},\Psi_{\text{saddle}}} = 0. \tag{132}$$

The third equation is given by the condition that the LPT goes through the saddle, i.e.

$$D(N_{\text{saddle}}, \Psi_{\text{saddle}}; F_{\text{crit}}) = 0. \tag{133}$$

Eq. (131) is the same as Eq. (125) and produces the same two roots as given in Eq. (128). However, it can be shown that $\Psi_{\text{saddle}} = \Psi_1$.

If $D_{\text{saddle}} < 0$, the level sets of $D = 0$ are not connected, they fall apart in two closed contours with values below N_{saddle} and another with values above N_{saddle}. At the moment the value D_{saddle} becomes 0 (cf. Fig. 3b), the two distinct contours unite and the trajectory reaches $N_{\max} = 1/2$, if condition (129) is also met. It is important to note that a saddle does not exist for all Δ values. Equation (132) yields

$$-\frac{2\sqrt{\varepsilon}}{3}\left(\frac{\Omega^2+1}{\Omega^2}\right)N_{\text{saddle}}^3 - \frac{8FN_{\text{saddle}}^2\varepsilon}{3\Omega^2\sqrt{4N_{\text{saddle}}^2\varepsilon + 9\Omega^2}} - 4\Delta N_{\text{saddle}} - \frac{3F}{\sqrt{4N_{\text{saddle}}^2\varepsilon + 9\Omega^2}} = 0, \tag{134}$$

where as Eq. (133) yields

$$\frac{(\Omega^2+1)N_{\text{saddle}}^4}{6\Omega^2}\sqrt{\varepsilon} + \frac{2N_{\text{saddle}}^2\Delta}{\Omega^2} + F_{\text{crit}}\cos(\Psi_1)N_{\text{saddle}} = 0 \tag{135}$$

Division of Eq. (135) by N_{saddle} and elimination of N_{saddle}^3 from Eqs. (134)–(135) yields the solution for F_{crit}

$$F_{\text{crit}}(N_{\text{saddle}}) = -\frac{12\Delta N_{\text{saddle}}\,\Omega^2\sqrt{4N_{\text{saddle}}^2\varepsilon + 9\Omega^2}}{8N_{\text{saddle}}^2\varepsilon + 27\Omega^2} \tag{136}$$

$$N_{\text{saddle}} = \frac{\sqrt{3}\sqrt{\varepsilon^{\frac{3}{2}}\sqrt{3}\sqrt{\Omega^2+1}\sqrt{-\varepsilon\left(128\Delta\sqrt{\varepsilon} - 27\Omega^2 - 27\right) - 9\varepsilon^2\left(\Omega^2+1\right)}\,\Omega}}{4\sqrt{\Omega^2+1}\,\varepsilon^{\frac{3}{2}}} \tag{137}$$

Insertion of Eq. (137) in Eq. (136) yields a very long expression that is difficult to interpret. However, a series expansion in ε yields the simple expression

$$F_{\text{crit,SM}} = \frac{8\Omega^2(-\Delta)^{3/2}}{3\sqrt{\Omega^2+1}}\varepsilon^{-1/4} + o(\varepsilon^{-1/4}), \tag{138}$$

defining the smallest values of the excitation amplitude dictated by the saddle mechanism.

E.3 Smallest possible force value leading to level crossing

The smallest possible force value causing the crossing of the critical level $N_{\max}$ is

$$F_{\text{crit,min}} = \frac{\Omega^2+1}{192\Omega}\sqrt{\varepsilon}, \text{ taken at } \Delta_{\min} = -\frac{\Omega^2+1}{64\Omega^2}\sqrt{\varepsilon}, \tag{139}$$

where the right branch of the maximum mechanism and the saddle mechanism intersect (cf. Fig. 4), which

is also the value of the frequency shift Δ where the right branch of the maximum mechanism becomes more significant than the saddle mechanism.

The left branch of the maximum mechanism is more significant than the saddle mechanism if $N_{\text{saddle}} > N_{\text{max}} = 1/2$, in which case reaching the saddle already implies reaching the critical level. This transition occurs at

$$\Delta_2 = -\frac{\left(\Omega^2+1\right)}{16\Omega^2}\sqrt{\varepsilon}, \tag{140}$$

with the critical force value

$$F_{\text{crit},2} = \frac{\left(\Omega^2+1\right)\sqrt{\varepsilon}}{24\Omega}. \tag{141}$$

Thus, the whole critical force amplitude curve is given by:

$$F_{\text{crit}}(\Delta) = \begin{cases} -\Delta\Omega - \frac{\Omega^2+1}{48\Omega}\sqrt{\varepsilon} & \text{for } \Delta < \Delta_2, \\ \frac{8\Omega^2(-\Delta)^{3/2}}{3\sqrt{\Omega^2+1}}\varepsilon^{-1/4} & \text{for } \Delta_2 < \Delta < \Delta_{\text{min}}, \\ \Delta\Omega + \frac{\Omega^2+1}{48\Omega}\sqrt{\varepsilon} & \text{for } \Delta_{\text{min}} < \Delta. \end{cases} \tag{142}$$

References

1. McPeek, M.A.: Coexistence in ecology: a mechanistic perspective, monographs in population biology, vol. 66 (Princeton University Press, Princeton, 2022). https://doi.org/10.2307/j.ctv1mjqw7t
2. Lotka, A.J.: Analytical Note on Certain Rhythmic Relations in Organic Systems. Proc. Natl. Acad. Sci. **6**(7), 410 (1920). https://doi.org/10.1073/pnas.6.7.410
3. Volterra, V.: Variazioni e fluttuazioni del numero d'individui in specie animali conviventi. Memoria della Reale Accademia Nazionale dei Lincei **2**, 31 (1926)
4. MacArthur, R.H.: Species packing, and what interspecies competition minimizes. Proc. Natl. Academy Sci. USA **64**, 1369 (1969)
5. MacArthur, R.H.: Species packing and competitive equilibrium for many species. Theor. Popul. Biol. **1**, 1 (1970)
6. MacArthur, R.H.: Geographical Ecology. Princeton University Press, Princeton (1972)
7. Du, Y., Niu, B., Wei, J.: Dynamics in a Predator-Prey Model with Cooperative Hunting and Allee Effect. Mathematics **9**(24), 3193 (2021). https://doi.org/10.3390/math9243193
8. Huang, Y., Zhu, Z., Li, Z.: Modeling the Allee effect and fear effect in predator-prey system incorporating a prey refuge. Adv. Diff. Equ. **2020**(1), 1 (2020). https://doi.org/10.1186/s13662-020-02727-5
9. Ikeda, M., Siljak, D.D.: In: 1979 18th IEEE conference on decision and control including the symposium on adaptive processes, vol. 2 (1979), pp. 593–601. https://doi.org/10.1109/CDC.1979.270250
10. Redheffer, R.: Nonautonomous Lotka-Volterra systems. I. J. Diff. Equ. **127**, 519 (1996). https://doi.org/10.1006/jdeq.1996.0081
11. Redheffer, R.: Nonautonomous Lotka-Volterra systems. II. J. Diff. Equ. **132**, 1 (1996). https://doi.org/10.1006/jdeq.1996.0168
12. Táboas, P.: Periodic solutions of a forced Lotka-Volterra equation. J. Math. Anal. Appl. **124**(1), 82 (1987). https://doi.org/10.1016/0022-247X(87)90026-6
13. Muhtar, N., Cahyono, E., Iswandi, R.M., Muhidin, M.: Lotka-Volterra Model with Periodic Harvesting. WSEAS Trans. Syst. **21**, 283 (2022). https://doi.org/10.37394/23202.2022.21.31
14. Nenciu, F., Voicea, I., Cocarta, D.M., Vladut, V.N., Matache, M.G., Arsenoaia, V.N.: "Zero-Waste" Food Production System Supporting the Synergic Interaction between Aquaculture and Horticulture. Sustainability **14**(20) (2022). https://doi.org/10.3390/su142013396
15. Puech, T., Stark, F.: Diversification of an integrated crop-livestock system: Agroecological and food production assessment at farm scale. Agric. Ecosyst. Environ. **344**, 108300 (2023). https://doi.org/10.1016/j.agee.2022.108300
16. Nutku, Y.: Hamiltonian Structure of the Lotka-Volterra Equations. Phys. Lett. A **145**(1), 27 (1990). https://doi.org/10.1016/0375-9601(90)90270-x
17. Plank, M.: Hamiltonian structures for the n-dimensional Lotka-Volterra equations. J. Math. Phys. **36**(7), 3520 (1995). https://doi.org/10.1063/1.531334
18. Landau, L., Lifshitz, E.: Mechanics, 3rd edn. Butterworth, Herrmann (1976)
19. Goldstein, H., Poole, C., Safko, J.: Class. Mech., 3rd edn. Pearson Education International, Upper Saddle River (2002)
20. Arnold, V.I.: Mathematical Methods of Classical Mechanics. Springer, Berlin (1989)
21. Percival, I., Richards, D.: Introduction to Dynamics. Cambridge University Press, Cambridge (1987)
22. Arnold, V., Kozlov, V., Neishtadt, A.: Mathematical Aspects of Classical and Celestial Mechanics. Springer, Berlin (2006)
23. Itin, A., Neishtadt, A., Vasiliev, A.: Captures into resonance and scattering on resonance in dynamics of a charged relativistic particle in magnetic field and electrostatic wave. Phys. D **141**, 281–296 (2000). https://doi.org/10.1016/S0167-2789(00)00039-7
24. Gendelman, O., Sapsis, T.: Energy exchange and localization in essentially nonlinear oscillatory systems: canonical formalism. J. Appl. Mech. Trans. ASME **84**, 1 (2017). https://doi.org/10.1115/1.4034930
25. Gendelman, O.: Escape of a harmonically forced particle from an infinite-range potential well: a transient resonance. Nonlinear Dyn. **93**, 79 (2018). https://doi.org/10.1007/s11071-017-3801-x
26. Gendelman, O., Karmi, G.: Basic mechanisms of escape of a harmonically forced classical particle from a potential well. Nonlinear Dyn. **98**, 2775 (2019). https://doi.org/10.1007/s11071-019-04985-9
27. Karmi, G., Kravetc, P., Gendelman, O.: Analytic exploration of safe basins in a benchmark problem of forced escape.

Nonlinear Dyn. **106**, 1573 (2021). https://doi.org/10.1007/s11071-021-06942-x
28. Farid, M.: Escape of a harmonically forced classical particle from asymmetric potential well. Commun. Nonlinear Sci. Numer. Simul. **84**, 1 (2020). https://doi.org/10.1016/j.cnsns.2020.105182
29. Farid, M.: Escape dynamics of a particle from a purely nonlinear truncated quartic potential well under harmonic excitation. Nonlinear Dyn. **111**(4), 3035 (2023). https://doi.org/10.1007/s11071-022-07976-5
30. Shih, S.D.: Comments on "A new method for the explicit integration of Lotka-Volterra equations". Divulgaciones Matemáticas **13**(2), 99 (2005). http://eudml.org/doc/52939
31. Boulnois, J.L.: An Exact Closed-Form Solution of the Lotka-Volterra Equations (2023)
32. Cahyono, E., Panre, M.A.B., Djafar, M.K.: A Second Order Solution of a Lotka-Volterra model near its equilibrium point. Eng. Lett. **32**(5), 1012 (2024)
33. Varma, V.: Exact solutions for a special prey-predator or competing species system. Bull. Math. Biol. **39**(5), 619 (1977). https://doi.org/10.1016/S0092-8240(77)80064-5
34. Waldvogel, J.: The Period in the Volterra-Lotka Predator-Prey Model. SIAM J. Numer. Anal. **20**(6), 1264 (1983). http://www.jstor.org/stable/2157163
35. Zaslavsky, G.M.: The Physics of Chaos in Hamiltonian Systems. Imperial College Press, London (2007)
36. Nayfeh, A.H., Mook, D.T.: Nonlinear Oscillations. Wiley, Hoboken (1995)
37. Manevitch, L.: New approach to beating phenomenon in coupled nonlinear oscillatory chains. Arch. Appl. Mech. **77**, 301 (2007)
38. Manevitch, L., Gendelman, O.: Tractable Modes in Solid Mechanics. Springer, Berlin (2011)
39. Manevitch, L.I.: A concept of limiting phase trajectories and description of highly non-stationary resonance processes. Appl. Math. Sci. **9**, 4269 (2014)
40. Kovaleva, A., Manevitch, L.: Autoresonance versus localization in weakly coupled oscillators. Physica D **320**, 1–8 (2014). https://doi.org/10.1016/j.physd.2016.01.001
41. Rega, G., Lenci, S.: Dynamical integrity and control of nonlinear mechanical oscillators. J. Vib. Control **14**, 159 (2008)
42. Nakamura, G.M., Martinez, A.S.: Hamiltonian dynamics of the SIS epidemic model with stochastic fluctuations. Sci. Rep. **9**(1), 15841 (2019). https://doi.org/10.1038/s41598-019-52351-x
43. Ballesteros, A., Blasco, A., Gutierrez-Sagredo, I.: Hamiltonian structure of compartmental epidemiological models. Physica D **413**, 132656 (2020). https://doi.org/10.1016/j.physd.2020.132656
44. Mező, I.: The Lambert W Function: Its Generalizations and Applications, 1st edn. (Chapman and Hall/CRC, 2022). https://doi.org/10.1201/9781003168102
45. Corless, R.M., Jeffrey, D.J., Knuth, D.E.: In: Proceedings of the 1997 international symposium on symbolic and algebraic computation (Kihei, HI) (ACM, New York, 1997), pp. 197–204. https://doi.org/10.1145/258726.258783